

The effects of bath gas and NO_x addition on n-pentane low-temperature oxidation in a jet-stirred reactor

Lorena Marrodán, Yu Song, Marco Lubrano Lavadera, Olivier Herbinet, Mara De Joannon, Yiguang Ju, Maria U. U. Alzueta, and Frédérique Battin-Leclerc

Energy Fuels, **Just Accepted Manuscript** • DOI: 10.1021/acs.energyfuels.9b00536 • Publication Date (Web): 30 Apr 2019

Downloaded from <http://pubs.acs.org> on May 8, 2019

Just Accepted

“Just Accepted” manuscripts have been peer-reviewed and accepted for publication. They are posted online prior to technical editing, formatting for publication and author proofing. The American Chemical Society provides “Just Accepted” as a service to the research community to expedite the dissemination of scientific material as soon as possible after acceptance. “Just Accepted” manuscripts appear in full in PDF format accompanied by an HTML abstract. “Just Accepted” manuscripts have been fully peer reviewed, but should not be considered the official version of record. They are citable by the Digital Object Identifier (DOI®). “Just Accepted” is an optional service offered to authors. Therefore, the “Just Accepted” Web site may not include all articles that will be published in the journal. After a manuscript is technically edited and formatted, it will be removed from the “Just Accepted” Web site and published as an ASAP article. Note that technical editing may introduce minor changes to the manuscript text and/or graphics which could affect content, and all legal disclaimers and ethical guidelines that apply to the journal pertain. ACS cannot be held responsible for errors or consequences arising from the use of information contained in these “Just Accepted” manuscripts.

The effects of bath gas and NO_x addition on *n*-pentane low-temperature oxidation in a jet-stirred reactor

Lorena Marrodán^{1#}, Yu Song^{2#}, Marco Lubrano Lavadera³, Olivier Herbinet², Mara de Joannon³, Yiguang Ju⁴, María U. Alzueta¹, Frédérique Battin-Leclerc²

¹Aragón Institute of Engineering Research (I3A), Department of Chemical and Environmental Engineering, University of Zaragoza, Spain.

²Laboratoire Réactions et Génie des Procédés, CNRS-Université de Lorraine, Nancy, France.

³Istituto di Ricerche sulla Combustione - C.N.R., Napoli – Italy.

⁴Department of Mechanical and Aerospace Engineering, Princeton University, NJ 08544, USA

Lorena Marrodán and Yu Song contributed equally.

Abstract

The oxidation of *n*-pentane (C₅H₁₂) in different bath gases (He, Ar, CO₂) and in Ar with NO₂ or NO addition has been studied in a jet-stirred reactor at 107 kPa, temperatures between 500-1100 K, with a fixed residence time of 2.0 s, under stoichiometric conditions. Four different quantification diagnostics were used: gas chromatography, chemiluminescence NO_x analyzer, continuous wave cavity ring-down spectroscopy, and Fourier transform infrared spectroscopy. The results showed that the onset temperature of the fuel reactivity was the same (575 K) regardless of the type of bath gases. Although the low-temperature fuel oxidation window was not affected by the type of bath gas, the *n*-pentane conversion was slightly larger when diluted in Ar through the negative temperature coefficient (NTC) region (625-725 K). Above 800 K, the reactivity according to the diluent was in the order CO₂ > Ar > He. In the presence of NO₂ or NO, it is found that the consumption rate of *n*-pentane exhibited a different trend below 700 K. The presence of NO₂ did not modify the fuel conversion below 675 K. In contrary, NO addition increased the onset temperature of the fuel reactivity by 75 K and almost no NTC zone was observed. This clearly indicated that NO addition inhibited *n*-pentane oxidation below 675 K. Above 700 K, *n*-pentane conversion was promoted by the presence of both NO_x additives. The intermediate species HONO was quantified and a search for HCN and CH₃NO₂ species was also

1 attempted. A new detailed kinetic mechanism was developed and allowed a good prediction of the
2 experimental data. Reaction rate and sensitivity analyses were conducted to illustrate the different
3 kinetic regimes induced by the NO_x addition. The inhibition by NO of the *n*-pentane oxidation below
4 675 K can be explained by its direct reaction with C₅H₁₁O₂ radicals disfavoring the classical promoting
5 channels via isomerizations, second O₂ addition and formation of ketohydroperoxides, the well-known
6 branching agents during alkane oxidation. With respect to NO₂ addition, the major consumption route
7 is via NO₂+CH₃=NO+CH₃O, which is not directly related to the direct fuel consumption. HONO
8 formation mainly derives from NO₂ reacting with CH_iO (i=2,3). The reaction, HONO+M =
9 OH+NO+M, is one of the most sensitive reactions for HONO depletion.

10
11
12
13
14
15
16
17
18
19
20
21
22
23 **Keywords:** Jet-stirred reactor; NO_x *n*-pentane combustion; bath gas; low-temperature oxidation.

24 25 26 27 **1. Introduction**

28
29
30 To meet the demand of stringent regulations, current engines are usually equipped with exhaust
31 gas recirculation (EGR), which shows significant advantage for emissions abatement ¹, because it
32 increases dilution and decreases the temperature in the combustion chamber.

33
34
35
36
37 When using EGR, the fuel combustion properties are altered by the presence of great amounts
38 of carbon dioxide and water induced by the recirculation of exhausted gases. Such species may have
39 both thermal and chemical effects on fuel oxidation ²⁻⁸. Lubrano Lavadera *et al.* ⁹ provided a summary
40 of the experimental and numerical studies made before 2016, which have investigated the effects of
41 CO₂ on combustion properties. They also observed that propane oxidation was significantly altered by
42 CO₂ addition in a jet-stirred reactor (JSR) at atmospheric pressure at temperatures between 720 and
43 900 K. They found that, at high temperatures, CO₂ inhibited the CO oxidation via the reactions CO₂ +
44 H = CO + OH and H + O₂ + M = HO₂ + M because of the high CO₂ three-body collisional efficiency.
45 Both reactions competed with the with the H + O₂ = OH + O reaction, diminishing the system reactivity.
46 Di *et al.* ¹⁰ studied the effects of different diluents, including Ar, N₂, and CO₂, on the low-temperature
47
48
49
50
51
52
53
54
55
56
57
58
59
60

1 ignition processes of *iso*-octane and *n*-heptane using a rapid-compression machine. The experimental
2 and modelling results confirmed that the bath gas composition had a significant impact on ignition
3
4 under conditions exhibiting two-stage ignition within the NTC region. However, the authors claimed
5
6 that the bath gas composition had little impact on the first-stage ignition at any of the conditions studied.
7
8 For temperatures below 800 K, the major impact of the buffer gas composition was due to thermal
9
10 effects. The chemical effect increased with increasing temperature. In the two aforementioned papers⁹,
11
12
13
14
15
16
17
18
19
20
21
22
23
24
25
26
27
28
29
30
31
32
33
34
35
36
37
38
39
40
41
42
43
44
45
46
47
48
49
50
51
52
53
54
55
56
57
58
59
60

Besides water and CO₂, NO_x (mainly NO and NO₂) are also present in significant amounts among the exhausted gases used in EGR. They play an important role in changing the reactivity of the fresh inlet fuel, and consequently in altering ignition delay times¹¹⁻¹⁵ and product emissions¹⁶⁻²⁷. A typical small-size component of gasoline surrogates is *n*-pentane. Many efforts were undertaken to study the oxidation of neat *n*-pentane oxidation²⁸⁻³⁴ or its role as a dual-fuel³⁵. However, reports in terms of the effect of NO_x addition on *n*-pentane oxidation are still scarce.

In 1996, Prabhu *et al.*³⁶ investigated the effect of NO addition on 1-pentene oxidation in a pressurized (6 atm) flow reactor between 600 and 800 K. Fuel reactivity and major products were determined using gas chromatography (GC) and Fourier transform infrared spectroscopy (FTIR). Despite this fuel was unsaturated, an alkane type behavior was observed for 1-pentene, with a NTC behavior, which was suppressed in presence of NO. No kinetic model was used to reproduce the experimental data. In 2005, Glaude *et al.*³⁷ proposed a detailed kinetic model for the mutual oxidation of NO and *n*-pentane at low-temperature in an atmospheric-pressure quartz flow reactor. They pointed out that the reactions of NO with HO₂ and with alkylperoxy (ROO) radicals releasing OH radical were responsible for the whole system oxidation acceleration. Recently, Zhao *et al.*^{38,39} studied the NO_x sensitization effects on *n*-pentane oxidation in an atmospheric JSR between 500 and 800 K. The fuel, both NO and NO₂ and several C₁-C₂ products were followed by electron impact molecular beam mass

1 spectrometry, μ GC and Faraday rotation spectrometry. The authors also developed a kinetic model to
2 explain the observed NTC retarding phenomenon in the presence of NO_x . They found HONO as an
3
4 important intermediate species during the oxidation process involving nitrogen containing species.
5
6

7
8 For atmospheric chemistry purpose, several attempts were made to identify and quantify
9 HONO⁴⁰⁻⁴². The absorption spectrum of HONO was first measured by Jain *et al.*⁴² with the aids of
10 continuous wave cavity ring-down spectroscopy (*cw*-CRDS). The cross section of HONO, which is
11 essential for its quantification, was determined. Regarding combustion studies, Chai and Goldsmith⁴³
12 calculated the rate coefficients for the H-abstraction reactions, H_2+NO_2 and CH_4+NO_2 , leading to the
13 formation of HONO. To the authors' best knowledge, during the oxidation of a fuel in the presence of
14 NO_x , HONO was only detected with *cw*-CRDS at CNRS-Nancy^{44,45}. In our first attempt, methane was
15 adopted to represent a biogas surrogate fuel in the presence of NO_x . It was found that HONO signals
16 were below the estimated/calculated detection limit (3 ppm)⁴⁴. More recently, HONO were
17 successfully identified and quantified during *n*-pentane JSR oxidation in presence of NO ⁴⁵.
18
19
20
21
22
23
24
25
26
27
28
29
30
31

32 In this context, following our previous work on neat *n*-pentane low-temperature oxidation
33 performed in an atmospheric JSR using GC and quantifying a wide range of $\text{C}_0\text{-C}_5$ products³⁰, we
34 present here a study of the effect of diluents (He, Ar, CO_2) and of NO_x addition on *n*-pentane oxidation
35 at temperatures ranging from 500 to 1100 K. NO_x species were followed by chemiluminescence, the
36 amount of HONO was quantified by means of *cw*-CRDS, and a search for intermediate species,
37 CH_3NO_2 and HCN, was made with the aid of FTIR. A new detailed kinetic mechanism was developed
38 and used to interpret the experimental data. The present study under stoichiometric conditions, with
39 different used bath gases and with a large range of analyzed species including HONO, will
40 significantly enlarge the data base already started by Zhao *et al.*^{38,39} on the same chemical system.
41
42
43
44
45
46
47
48
49
50
51

52 2. Experimental setup

53 The experimental setup used was a laboratory-scale spherical fused silica JSR (volume of 81.2
54 cm^3 ; detailed description provided elsewhere⁴⁶). The liquid *n*-pentane was filled into a tank and
55
56
57
58
59
60

1
2 pressurized with He. The flow rate of *n*-pentane was controlled by a Coriolis flow controller. After the
3
4 evaporation in a heat exchanger, the gaseous *n*-pentane, along with the gas diluent and oxygen, was
5
6 premixed before entering in an annular preheating zone and to the reactor afterward through four
7
8 different nozzles. These nozzles created high turbulence, which results in homogeneous distributions
9
10 of mixture compositions and temperature in the reactor. The residence time inside the preheating zone
11
12 was only $\approx 1\%$ with respect to that in the reactor, which was kept fixed at 2.0 s (± 0.1 s) within all the
13
14 experiments performed. Both the reactor and the preheating zone were heated using Thermocoax
15
16 resistances.
17
18

19
20 The reactor temperature was measured by a type-K thermocouple (± 5 K) located at the center
21
22 of the reactor. The pressure in the reactor was controlled by a needle valve (± 0.2 kPa) positioned
23
24 downstream of the reactor and kept constant at 107 kPa (800 Torr). Argon, helium, carbon dioxide,
25
26 oxygen, NO, and NO₂ were provided by Messer (purities of 99.99%, respectively). The flow rates of
27
28 the gases were controlled by mass flow controllers ($\pm 0.5\%$).
29
30

31 The gases leaving the reactor were analyzed on-line using four analytical techniques:

- 32
33 • Three gas chromatographs were equipped with three columns (carbosphere packed column,
34
35 PlotQ capillary column, and a HP-5 capillary column), a TCD (thermal conductivity detector) and an
36
37 FID (flame ionization detector). The previous product identification made using a GC-MS operating
38
39 with electron ionization³⁰ was also used in the present work.
40
41
- 42
43 • A chemiluminescence NO_x analyzer (Thermo Scientific Model 42i) was adopted to measure
44
45 NO and NO₂. The quantitative range is 0-5000 ppm for NO and 0-500 ppm for NO₂ with 0.1 ppm
46
47 sensitivity, respectively. Two pumps were used for outlet and bypass channels, respectively.
48
49
- 50
51 • An FTIR spectrometer (Thermo Scientific Antaris) was used to detect the CH₃NO₂ (if any) and
52
53 HCN (if any) species, see more details in⁴⁴.
54
55
- 56
57 • A home-made *cw*-CRDS infrared spectroscopy was used to detect H₂O, CH₂O and HONO
58
59 species, the description of this instrument is also provided in⁴⁷.
60

1
2 The uncertainty in the species concentration measurements using the different diagnostic instrument
3
4 is estimated to be $\pm 5\%$, except for the FTIR and CRDS measurements, for which it can be estimated
5
6 as $\pm 10\text{-}15\%$.
7

9 **3. Kinetic Model**

11
12 The new chemical kinetic mechanism developed in the present work includes the *n*-pentane
13
14 mechanism previously developed by the Galway group and successfully used in previous *n*-pentane
15
16 oxidation studies^{30,31}, and an updated C₀-C₁ NO_x sub-mechanism from the Princeton group³⁸. This
17
18 last sub-mechanism already contains reactions of C₅ alkoxy radicals with NO to produce aldehydes
19
20 and HNO. Additional reactions to merge/join the *n*-pentane mechanism and the NO_x sub-mechanism
21
22 are included in our new mechanism. The added reactions shown in Table 1 are written by analogy with
23
24 the work of Glaude *et al.*³⁷ for *n*-pentane/*n*-butane oxidation in the presence of NO, and that of
25
26 Anderlohr *et al.*⁴⁸ for the oxidation of engine surrogate fuels (*n*-heptane, *iso*-octane and toluene) in
27
28 the presence of NO.
29
30
31

32
33 The added reactions include the reactions of C₂-C₅ alkyl radicals with NO₂ to give NO and the
34
35 corresponding alkoxy radicals. The kinetic parameters for those reactions were taken similar to those
36
37 proposed by Glarborg *et al.*⁴⁹ for the reaction $\text{CH}_3 + \text{NO}_2 = \text{CH}_3\text{O} + \text{NO}$ (with an uncertainty around a
38
39 factor of 2).
40

41
42 The C₂-C₅ peroxy radicals can react with NO to also produce the corresponding alkoxy radicals;
43
44 in the case of hydroperoxy peroxypropyl radicals, the decomposition of the alkoxy radicals in
45
46 formaldehyde, propene and hydroxyl radical is directly written. The abstractions by NO₂ of H-atoms
47
48 from *n*-pentane and of the aldehydic H-atom from C₂-C₅ aldehydes leading to HONO are also
49
50 considered. Alkyl radicals can react with HNO to give NO and the corresponding alkanes. Finally, the
51
52 combinations between alkyl radicals and NO₂ are also written.
53
54
55
56
57
58
59
60

Table 1. Reactions included to join both Galway and Princeton mechanisms. Kinetic parameters of the form $k=A \times T^n \times \exp(-E_a/RT)$. Units: A is in cm^3 , mol, and s; E_a is in cal/mol.

Reaction	A	n	E_a	Source
$\text{R}\cdot + \text{NO}_2 = \text{RO}\cdot + \text{NO}^{\text{a}}$	4.00×10^{13}	-0.2	0	48
$\text{C}_2\text{H}_5\cdot + \text{NO}_2 = \text{NO} + \text{C}_2\text{H}_5\text{O}\cdot$	4.00×10^{13}	-0.2	0	49
$\text{C}_3\text{H}_7\cdot + \text{NO}_2 = \text{NO} + \text{C}_3\text{H}_7\text{O}\cdot^{\text{b}}$	4.00×10^{13}	-0.2	0	49
$\text{C}_4\text{H}_9\cdot + \text{NO}_2 = \text{NO} + \text{C}_4\text{H}_9\text{O}\cdot^{\text{b}}$	4.00×10^{13}	-0.2	0	49
$\text{RO}_2\cdot + \text{NO} = \text{RO}\cdot + \text{NO}_2^{\text{a}}$	2.53×10^{12}	0.0	-358	50
$\text{C}_2\text{H}_5\text{O}_2\cdot + \text{NO} = \text{C}_2\text{H}_5\text{O}\cdot + \text{NO}_2$	2.53×10^{12}	0.0	-358	50
$\text{C}_3\text{H}_7\text{O}_2\cdot + \text{NO} = \text{C}_3\text{H}_7\text{O}\cdot + \text{NO}_2^{\text{b}}$	2.53×10^{12}	0.0	-358	50
$\text{C}_4\text{H}_9\text{O}_2\cdot + \text{NO} = \text{C}_4\text{H}_9\text{O}\cdot + \text{NO}_2^{\text{b}}$	2.53×10^{12}	0.0	-358	50
$\cdot\text{OOQOOH} + \text{NO} = 2\text{CH}_2\text{O} + \text{C}_3\text{H}_6 + \text{NO}_2 + \text{OH}^{\text{a}}$	4.70×10^{12}	0.0	-358	48
$\text{CH}_3\text{CHO} + \text{NO}_2 = \text{CH}_3\cdot + \text{CO} + \text{HONO}$	8.35×10^{-11}	6.68	8300	48
$\text{C}_2\text{H}_5\text{CHO} + \text{NO}_2 = \text{C}_2\text{H}_5\cdot + \text{CO} + \text{HONO}$	8.35×10^{-11}	6.68	8300	48
$\text{C}_3\text{H}_7\text{CHO} + \text{NO}_2 = \text{C}_3\text{H}_7\cdot + \text{CO} + \text{HONO}^{\text{b}}$	8.35×10^{-11}	6.68	8300	48
$\text{C}_4\text{H}_9\text{CHO} + \text{NO}_2 = \text{C}_4\text{H}_9\cdot + \text{CO} + \text{HONO}^{\text{b}}$	8.35×10^{-11}	6.68	8300	48
$\text{Y}\cdot + \text{NO}_2 = \text{acrolein} + \text{R}'\cdot + \text{NO}^{\text{c}}$	2.35×10^{13}	0.0	0.0	52
$\text{RH} + \text{NO}_2 = \text{R}\cdot + \text{HONO}^{\text{a,d}}$	$(\alpha) 2.2 \times 10^{13}$	0.0	31100	53
	$(\beta) 5.8 \times 10^{12}$	0.0	28100	
$\text{R}\cdot + \text{HNO} = \text{NO} + \text{RH}^{\text{a,e}}$	1.47×10^{11}	0.76	349	54
$\text{C}_2\text{H}_5\cdot + \text{HNO} = \text{NO} + \text{C}_2\text{H}_6^{\text{e}}$	1.47×10^{11}	0.76	349	54
$\text{C}_3\text{H}_7\cdot + \text{HNO} = \text{NO} + \text{C}_3\text{H}_8^{\text{b,e}}$	1.47×10^{11}	0.76	349	54
$\text{C}_4\text{H}_9\cdot + \text{HNO} = \text{NO} + \text{C}_4\text{H}_{10}^{\text{b,e}}$	1.47×10^{11}	0.76	349	54
$\text{RNO}_2 (+\text{M}) = \text{R}\cdot + \text{NO}_2 (+\text{M})^{\text{a}}$ (high pressure)	1.80×10^{17}	0.0	58500	48
Fall off Parameter $F_c = 0.183$ (low pressure)	1.3×10^{18}	0.0	42000	
$\text{C}_2\text{H}_5\text{NO}_2 (+\text{M}) = \text{C}_2\text{H}_5\cdot + \text{NO}_2 (+\text{M})$ (high pressure)	1.80×10^{17}	0.0	58500	48
Fall off Parameter $F_c = 0.183$ (low pressure)	1.3×10^{18}	0.0	42000	
$\text{C}_3\text{H}_7\text{NO}_2 (+\text{M}) = \text{C}_3\text{H}_7\cdot + \text{NO}_2 (+\text{M})^{\text{b}}$ (high pressure)	1.80×10^{17}	0.0	58500	48
Fall off Parameter $F_c = 0.183$ (low pressure)	1.3×10^{18}	0.0	42000	
$\text{C}_4\text{H}_9\text{NO}_2 (+\text{M}) = \text{C}_4\text{H}_9\cdot + \text{NO}_2 (+\text{M})^{\text{b}}$ (high pressure)	1.80×10^{17}	0.0	58500	48
Fall off Parameter $F_c = 0.183$ (low pressure)	1.3×10^{18}	0.0	42000	

^a $\text{R}\cdot$, $\text{RO}\cdot$, $\text{ROO}\cdot$ and $\cdot\text{OOQOOH}$ are pentyl radical isomers, and the derived alkoxy, pentylperoxy and hydroperoxy peroxy pentyl radicals, respectively.

^b For $\text{C}_3\text{H}_7\cdot$ and $\text{C}_4\text{H}_9\cdot$, both linear isomers are considered.

^c $\text{Y}\cdot$ are the C_3 - C_5 resonance-stabilized alkenyl radicals considered in the *n*-pentane model, $\text{R}'\cdot$ is an H-atom or a C_1 - C_2 alkyl radicals.

^d α : kinetic parameters per primary H-atom, β : kinetic parameters per secondary H-atom,

^e The rate constant has been taken as equal to that of reaction $\text{CH}_3 + \text{HNO} = \text{CH}_4 + \text{NO}$.

Moreover, the chemistry of HONO is also updated by the adoption of the rate constant for $\text{NO} + \text{OH} (+\text{M}) = \text{HONO} (+\text{M})$ ⁵⁵, along with a modified third-body coefficient for Ar (coefficient of 0.1). The kinetic parameters for the HONO forming reaction ($\text{NO}_2 + \text{HO}_2 = \text{HONO} + \text{O}_2$) are adopted following Rasmussen *et al.*²² and those of the reaction associated with OH radical attacking HONO to form NO_2 and H_2O is implemented following Burkholder *et al.*⁵⁶. Two channels are considered for the reaction of HNO with NO_2 , one giving HNO_2 and NO and another producing $\text{HONO} + \text{NO}$.

The complete mechanism, which involves 832 species and includes 4218 reactions, is provided as Supplementary Material of this paper in CHEMKIN format, along with thermodynamic properties. The thermodynamic data for the involved species have been taken from the same sources as in the two original mechanisms^{30, 38}. The present mechanism is able to reproduce experimental data from literature^{38, 39} as shown in Fig. S1-S.4 in the Supplementary Material.

4. Results

The experiments for the neat *n*-pentane oxidation with different bath gases (He, Ar, CO_2) and for the oxidation of *n*-pentane doped with NO and NO_2 diluted in argon were carried out under stoichiometric conditions over the 500-1100 K temperature range. Equivalence ratios were calculated neglecting the amounts of added NO_x compounds, which were around 4-10% that of *n*-pentane (this to keep the inlet fuel and oxygen mole fractions constant in all experiments). The experimental conditions investigated in this study are presented in Table 2. A spreadsheet including all the experimental data, including N-atom balance, is provided in Supplementary Material.

Table 2. Experimental conditions (T=500-1100 K; P=107 kPa; residence time 2 s; X_i is the mole fraction of species i)

Exp.	$X_{n\text{-pentane}}$	X_{NO} ppm	X_{NO_2} ppm	X_{O_2}	Φ	Bath gas
1	0.01	-	-	0.08	1	Ar
2	0.01	-	-	0.08	1	He
3	0.01	-	-	0.08	1	CO_2
4	0.01	1000	-	0.08	1	Ar
5	0.01	500	-	0.08	1	Ar
6	0.01	-	400	0.08	1	Ar

1 Numerical calculations were conducted with the CHEMKIN-PRO software package ⁵⁷.
2
3
4 Transient solver was applied in the simulation tasks with sufficient time allowed to reach the steady
5
6 state solution.
7

8 **4.1 Experimental results and comparison with simulations**

9
10 In this part, we present the experimental results obtained first for the different used bath gases,
11 and then with the addition of NO_x. In both cases, the experimental results are compared to predictions
12 using the aforementioned model. In all the figures shown in this part, experimental results are denoted
13 by symbols, and simulations by lines.
14
15
16
17
18

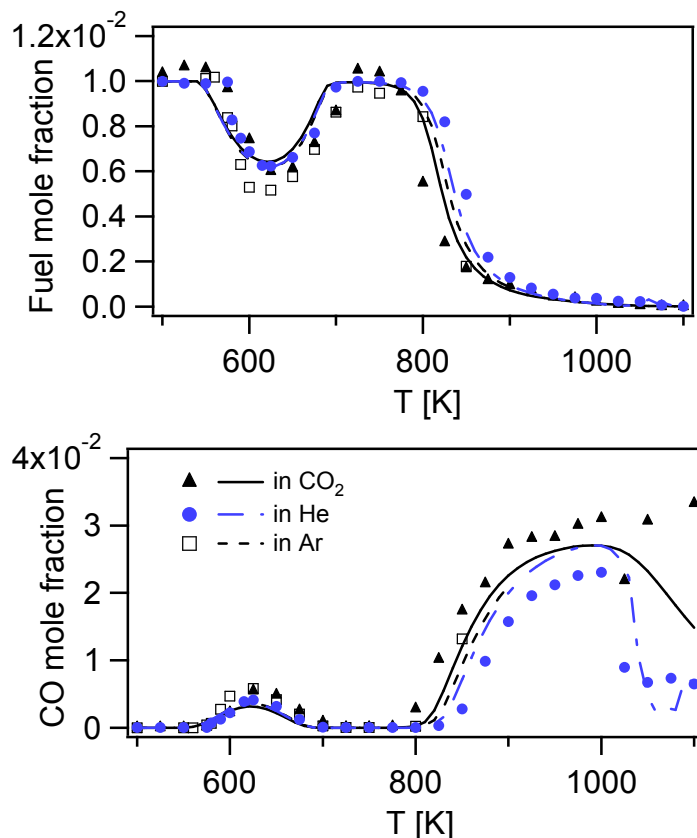
19 *4.1.1 The oxidation of neat n-pentane: the effect of different bath gases*

20
21 Figure 1 shows the temperature dependence between 500 and 1100 K of the mole fractions of
22 *n*-pentane and CO using the three different bath gases, Ar, He, and CO₂ (Exp. 1-3 in Table 2). The
23 temperature of the reactivity onset is approximately 575 K, regardless of the bath gas. As temperature
24 increases to 625 K, the starting temperature of the NTC zone, the conversion of *n*-pentane with Ar as
25 the carrier gas is slightly larger than that when using He and CO₂. However, *n*-pentane is more reactive
26 with CO₂ as the carrier gas compared to He and Ar over the temperature range between 800-900 K.
27 For CO mole fraction, in the 850-1000 K temperature range, modelling predictions do not show as
28 much influence of the carrier gas as it can be seen in the experimental results.
29
30
31
32
33
34
35
36
37
38
39
40

41 At the highest temperatures, the CO amount is the largest for the CO₂ diluted mixtures. Note
42 that dynamic behaviors (oscillations) occur when temperature is above 850 K with Ar as a carrier gas,
43 which explains why the data, neither experimental nor modeling with Ar are shown in Figure 1 above
44 this temperature. Oscillation regime was already observed and numerically predicted in previous
45 studies with methane as fuel⁵⁸; this is also an interesting topic of research, but beyond the goals of the
46 present work.
47
48
49
50
51
52
53

54 The kinetic mechanism is able to reproduce the experimental data although the mole fraction
55 of *n*-pentane is slightly overestimated at 625 K with Ar as the carrier gas. Below 800 K, the model
56
57
58
59
60

1 predicts the same *n*-pentane conversion trend for He and Ar, and a slightly lower conversion for CO₂.
2
3
4 With respect to the CO formation, the model underestimates it with CO₂ as the bath gas when
5
6 temperature is above 1050 K.
7
8
9



37 Figure 1: Temperature dependence of *n*-pentane and CO mole fraction with different bath
38 gases. Symbols are experiments, lines simulations.
39

40 Because the temperature is assumed to be uniform inside the reactor, the reactivity differences
41 for different bath gases observed above 800 K might be ascribed rather to different third body
42 coefficients than to the different heat release rates due to thermal diffusion heat transfer rates under
43 the different bath gas environments. The branching mechanism represented by the reaction $\text{H}_2\text{O}_2 (+\text{M})$
44 $= \text{OH} + \text{OH} (+\text{M})$ is altered in virtue of the higher collisional efficiencies of CO₂ with respect to Ar
45 and He. This is consistent with what was previously observed in ⁹. At the highest temperatures, the
46 reaction $\text{CO}_2 + \text{H} = \text{CO} + \text{OH}$ explains why the CO amount is largest for the CO₂ diluted mixtures.
47
48
49
50
51
52
53
54
55
56
57
58
59
60

4.1.2 The oxidation of *n*-pentane doped with NO_x .

The results obtained between 500 and 900 K in the absence and in the presence of NO_x are presented in Figure 2.

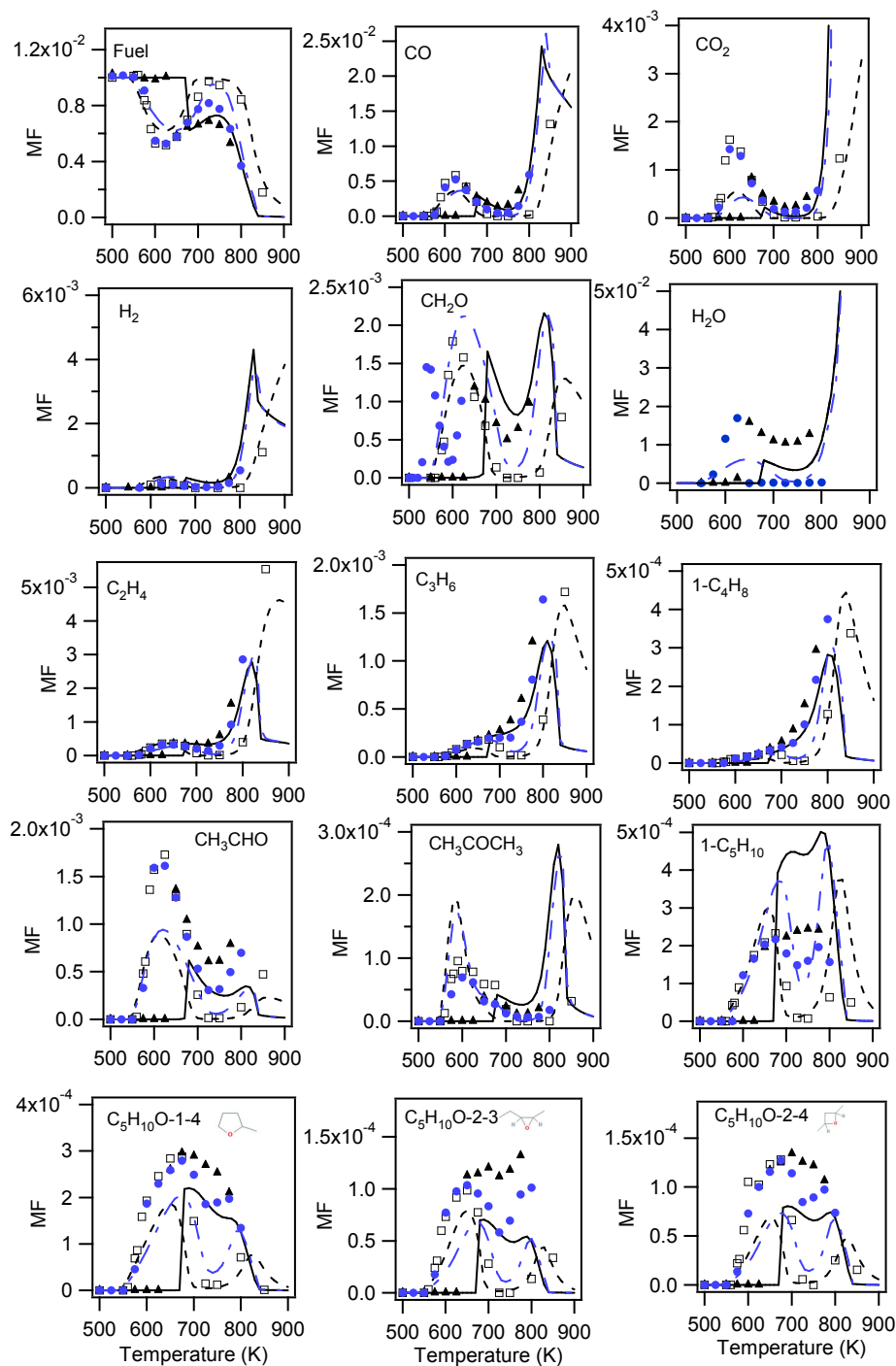


Figure 2: Influence of NO_x addition (with Ar as bath gas) on the mole fractions (MF) of *n*-pentane and of its main oxidation products. Symbols are experiments, lines simulations (empty squares and broken lines: no additive, black triangles and full lines: + NO, blue rounds and mixed lines: + NO_2).

1
2
3 In all the experiments with NO_x addition, the carrier gas is Ar (Exp. 5 and 6 in Table 2). Besides
4 the temperature dependence of *n*-pentane mole fractions, the formation of some of the major reaction
5 products are also displayed.
6
7
8

9
10 As it can be seen, the addition of 500 ppm NO (triangles) has a strong effect on the *n*-pentane
11 reactivity. The onset temperature for *n*-pentane is shifted from 575 K to 625 K by the addition of NO.
12 This fact indicates that the presence of NO inhibits the reactivity of *n*-pentane in the NTC region.
13 Above 700 K, the *n*-pentane conversion is larger in presence of NO compared to the other two cases.
14 On the other hand, the presence of 400 ppm NO₂ (circles), does not considerably modify the *n*-pentane
15 mole fraction below 700 K. Above this temperature, the *n*-pentane conversion in the presence of NO₂
16 is in between that with added NO and that with neat *n*-pentane (squares).
17
18
19
20
21
22
23
24

25
26 With NO addition, the initial temperature for the formation of the main oxidation products,
27 such as CO, H₂, C₂H₄, C₃H₆, 1-butene, 1-pentene, formaldehyde, acetaldehyde, acetone, and cyclic
28 ethers (C₅H₁₀O-1-4 [2-methyltetrahydrofuran], C₅H₁₀O-2-4 [2,4-dimethyloxetane] and C₅H₁₀O-2-3
29 [methyl-ethyl-oxirane]), increases up to 650 K. For the products exhibiting a NTC area in neat mixtures,
30 this behavior is significantly reduced in presence of NO. NO₂ addition does not much alter the product
31 formation below 700 K.
32
33
34
35
36
37
38

39
40 Overall, there is a good agreement between experimental data and model predictions, especially
41 for light hydrocarbon species (C₂H₄, C₃H₆, and 1-C₄H₈). Moreover, the model can also predict quite
42 well the profiles of H₂ and formaldehyde. More deviations are encountered for acetaldehyde and
43 acetone. H₂O formation (not measured without additive) is also underestimated by the model, which
44 was also observed in the previous methane and NO_x low temperature oxidation work⁴⁴. It might be
45 ascribed to the uncertainty in cw-CRDS measurements because of its significant mole fraction.
46 Regarding C₅ species, the model overestimates the mole fraction of 1-pentene and underestimates that
47 of cyclic ethers. However, the difference in the shape of the temperature dependence profiles between
48 neat mixture and with NO_x addition is well reproduced. As is shown by experiments, the strong mole
49
50
51
52
53
54
55
56
57
58
59
60

fraction decrease predicted between 700 and 800 K in neat mixture or with NO₂ addition, almost completely disappears with added NO.

In order to evaluate the effect of the amount of added NO on the *n*-pentane oxidation, one more set of experiments in the presence of 1000 ppm NO was studied (Exp. 4 in Table 2). As is shown in Figure 3, in the case of 1000 ppm of NO (blue circles), the onset temperature for *n*-pentane conversion is shifted from 625 K (500 ppm of NO) to 675 K. This implies that the retarding effect of NO on *n*-pentane oxidation is even stronger with the increase of the amount of added NO. Once the reaction is started, as temperature increases, the consumption of *n*-pentane is larger in the presence of 1000 ppm NO than that with only 500 ppm NO addition.

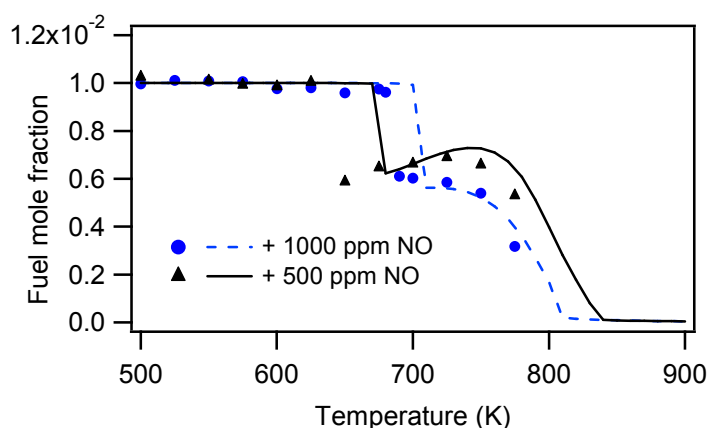


Figure 3: Mole fractions of *n*-pentane in the presence of NO (500 or 1000 ppm). Symbols are experiments, lines simulations.

Figure 4 shows the temperature dependence of NO, NO₂ and HONO mole fractions in the presence of NO and NO₂. When its initial mole fraction is 500 ppm, NO starts to be consumed at 625 K, in the meanwhile, the mole fraction of NO₂ increases sharply to reach approximately 300 ppm. Above 650 K, NO is fully consumed, and the amount of NO₂ continues gradually increasing until 750 K. Concerning HONO, for which the quantification procedure under oxidation process was demonstrated elsewhere⁴⁵, its produced mole fraction is nearly 100 ppm at a temperature of 650 K.

The HONO mole fraction also increases until the temperature is 725 K. After that, it decays as the temperature further increases.

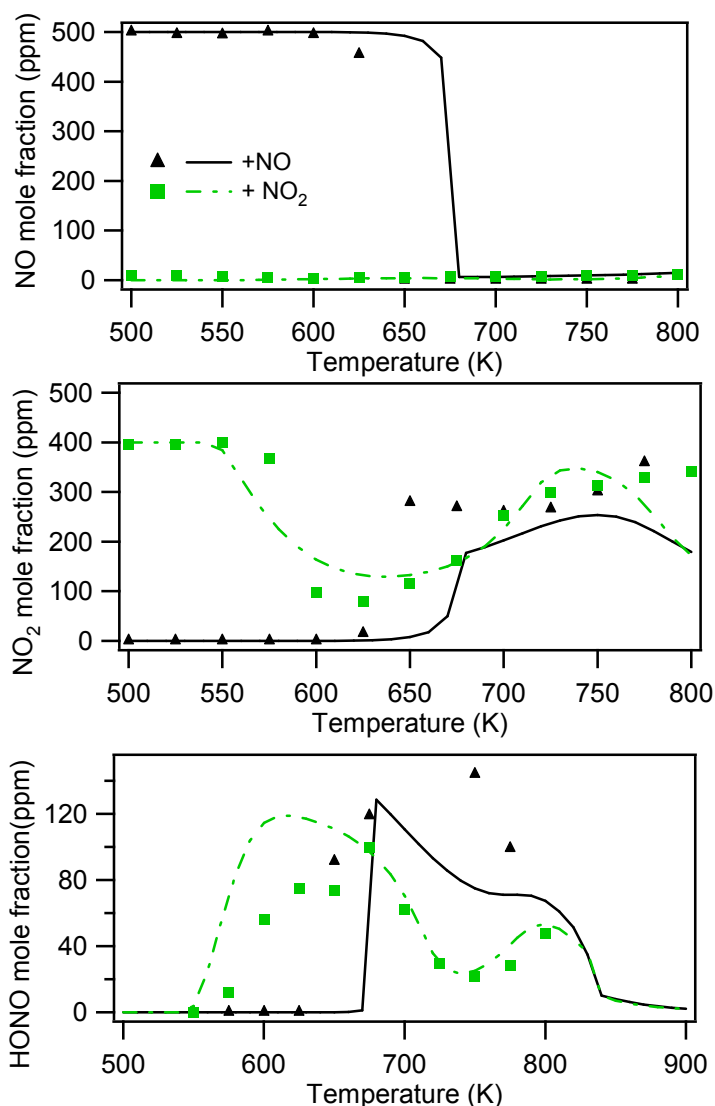


Figure 4: Temperature dependence of NO, NO₂ and HONO mole fractions in the presence of NO (500 ppm) or NO₂ (400 ppm). Symbols are experiments, lines simulations.

When NO₂ (400 ppm) is added as a reactant, the onset temperature for its consumption is approximately 575 K, which is consistent with that of neat *n*-pentane as is shown in Figure 2. The NO₂ mole fraction drops to 90 ppm at a temperature of 625 K, then it increases again with the increase of temperature. HONO mole fraction gradually increases to 120 ppm when the temperature is 675 K. After

1 that, the amount of HONO decreases to 70 ppm at 800 K. No NO formation is observed in the case of
2
3
4 NO₂ addition, as it can be seen in the upper part of Figure 4.
5

6 With the aids of FTIR, a search for HCN (detection limit of 100 ppm⁴⁴) and CH₃NO₂ (detection
7
8 limit of 5 ppm⁴⁴) species was attempted. However, there was no obvious signal of these two species
9
10 on the spectra when compared to the standard ones at all the studied temperatures. The nitrogen mass
11
12 balance significantly deteriorates in the temperature range from 600 to 700 K, this lack of nitrogen
13
14 might be partly due to the detection limits of the current diagnostic instruments, but this is not fully
15
16 understood.
17
18

19
20 The model captures satisfactorily the experimental trends for NO mole fractions. It slightly
21
22 overestimates the amount of HONO when the temperature is below 650 K in the presence of NO, and
23
24 in the case of NO₂ addition when the temperature is above 650 K. Regarding NO₂ addition, the model
25
26 underestimates the produced mole fraction of NO₂ when the temperature is above 750 K. Note that the
27
28 model predicts the formation of CH₃NO₂ and C₂H₅NO₂ in the presence of NO_x, especially in the 600-
29
30 700 K temperature range, while none of these species was observed from an experimental point of
31
32 view (the features present in the C₂H₅NO₂ FTIR spectrum of the NIST WebBook database⁵⁹ were not
33
34 observed in our FTIR spectra). Simulations did not show notable amounts of HCN, but a maximum
35
36 mole fraction of 40 ppm was predicted for CH₃NO₂ in presence of NO and of 70 ppm in presence of
37
38 NO₂. Note that a notable formation of C₂H₅NO₂ was also predicted, with a maximum mole fraction of
39
40 130 ppm in presence of NO, and of 95 ppm in presence of NO₂. More studies on the reactions of
41
42 CH₃NO₂ and C₂H₅NO₂ would certainly be helpful to improve the model.
43
44
45
46

47 **5. Discussion**

48
49 Reaction rate and sensitivity analyses were performed to clarify the different reaction paths for
50
51 the oxidation of *n*-pentane with and without NO_x addition. Especially, the different low-temperature
52
53 *n*-pentane oxidation behaviors with both NO and NO₂ addition, and the HONO formation route were
54
55 analyzed. A first characteristic temperature of 625 K, which is the typical of the low-temperature
56
57
58
59
60

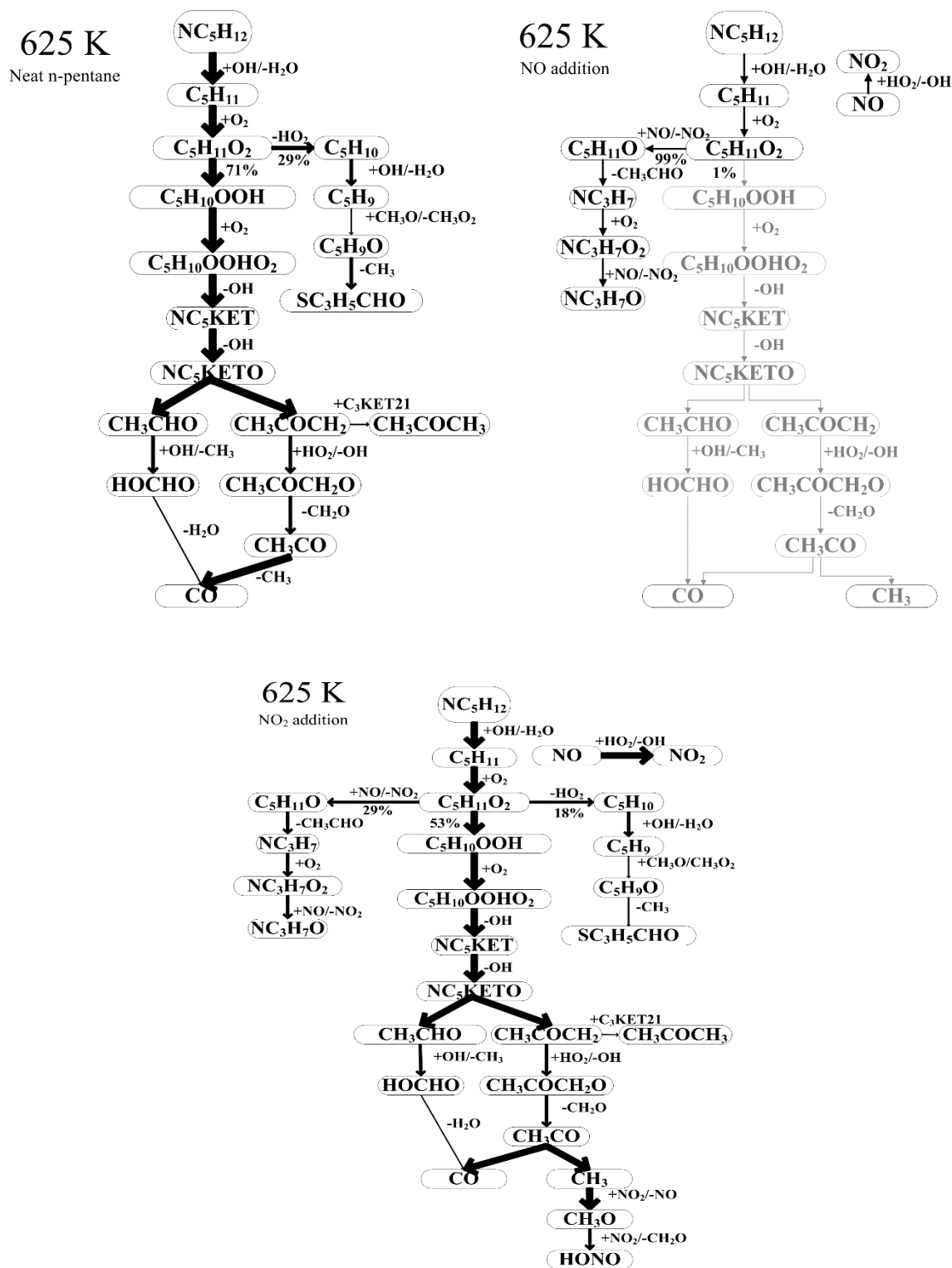


Figure 5: Reaction path diagram for *n*-pentane oxidation with or without NO_x addition at 625 K. The thickness of the arrow represents the flow rate of the corresponding reactions.

1 oxidation area, was selected to perform this analysis. The reaction paths for *n*-pentane consumption at
2 this temperature are shown in Figure 5.
3
4

5
6 In the absence of NO_x, the *n*-pentane oxidation starts by H-abstractions by OH radicals.
7
8 Depending on the H-abstraction site, three different pentyl radicals can be produced, although C₅H₁₁-2
9 is the predominant one. These pentyl radicals react with molecular oxygen to form C₅H₁₁O₂ radicals,
10 which could readily isomerize to give C₅H₁₀OOH radicals, even at this relatively low temperature.
11 C₅H₁₀OOH radicals then again add to O₂ and are a source of OH radicals and ketohydroperoxides,
12 well-known branching agents. The decomposition of main ketohydroperoxide obtained starting from
13 C₅H₁₁-2 produces OH, CH₃CHO and CH₃COCH₂. These last two species lead to the formation of
14 CH₂O, acetone, and CO. The released OH radicals could then react again with reactant, *n*-pentane.
15 This sequence of reactions acts as a branching process, multiplying the number of radicals, therefore
16 accelerating the whole system.
17
18
19
20
21
22
23
24
25
26
27
28

29 In presence of NO, the route starting by the isomerization of C₅H₁₁O₂ to C₅H₁₀OOH radicals,
30 which are marked in grey in Fig. 5, becomes almost negligible. Instead, with the aid of NO, C₅H₁₁O₂
31 converts to C₅H₁₁O radicals. This explains why, under these conditions, *n*-pentane is barely consumed
32 as is shown in Fig.2. C₅H₁₁O radical decomposes to relatively unreactive species, CH₃CHO and NC₃H₇
33 radicals, compared to the highly reactive OH radicals derived from the presence of NO. Therefore, the
34 route starting by the isomerization of C₅H₁₁O₂ to C₅H₁₀OOH radicals, which is marked in grey in
35 Figure 5, becomes almost negligible. It can be concluded that the self-sustained oxidation process with
36 the help of OH radicals, formed in branching chains, is significantly disturbed by the addition of NO.
37
38
39
40
41
42
43
44
45
46
47

48 In presence of NO₂, the major consumption route for NO₂ is NO₂+CH₃=NO+CH₃O, which has
49 a minor direct effect on the *n*-pentane oxidation. Consequently, the *n*-pentane conversion displays a
50 similar trend as that for the neat *n*-pentane as shown in Figure 2. Methyl radicals are produced via the
51 ketohydroperoxide decomposition route. Meanwhile, the generated NO can somehow reduce the
52 reactivity of the system as mentioned above. However, this effect is compensated by the fact that NO
53
54
55
56
57
58
59
60

1
2 could convert back to NO_2 with the aids of HO_2 , releasing OH radical ($\text{NO} + \text{HO}_2 = \text{NO}_2 + \text{OH}$), which
3
4 can accelerate the *n*-pentane oxidation. Note that NO_2 can react with CH_3O radical to form HONO and
5
6 CH_2O ($\text{NO}_2 + \text{CH}_3\text{O} = \text{HONO} + \text{CH}_2\text{O}$) explaining why, at 625 K, HONO is formed in presence of NO_2 ,
7
8 and not with NO, as is shown in Figure 4.
9

10
11 At an intermediate temperature of 725 K, the initial consumption route of neat *n*-pentane is
12
13 still provided by the OH radical attack. However, once the $\text{C}_5\text{H}_{11}\text{O}_2$ radicals are generated, the main
14
15 consumption route switches to decompose them directly to pentenes and HO_2 radicals. These last
16
17 species are relatively stable and their formation competes with the branching route via
18
19 ketohydroperoxides. Consequently, the fuel reactivity is dramatically hindered, and *n*-pentane mole
20
21 fraction almost rebounds to the initial input value (See Figure 2). When added, NO can react with the
22
23 abundant HO_2 radicals, regenerating active OH radicals, which can accelerate the *n*-pentane oxidation.
24
25 This explains why the *n*-pentane consumption keeps significant from 675 to 725 K (See Figure 2).
26
27 With respect to HONO, the formed NO_2 can further react with CH_3O and HO_2 radicals, along with
28
29 CH_2O to form HONO, which can explain the high amount of HONO experimentally detected at 675 K.
30
31 At the same temperature but in the presence of NO_2 , the NO- HO_2 interaction cannot so easily induce
32
33 additional OH radicals formation and the temperature dependence of *n*-pentane mole fraction displays
34
35 a similar trend compared to the neat *n*-pentane oxidation. In terms of HONO, its formation route is
36
37 similar as that in the case of NO addition, however, the mole fraction of HONO is lower than that in
38
39 the presence of NO; it might be ascribed to the lower initial mole fraction of NO_2 addition (400 ppm)
40
41 compared to the NO addition (500 ppm).
42
43
44
45
46

47
48 The flow rate analysis displayed in Figure 6 was performed at a temperature of 775 K. The
49
50 reaction paths, which are enclosed in the dash box, belong to the common *n*-pentane consumption
51
52 routes with or without NO_x addition. Note that, at this temperature, the importance of the channels
53
54 associated with the *n*-pentane low-temperature oxidation are less important. The reactions of pentyl
55
56 radicals by β -scission reactions ($\text{C}_5\text{H}_{11}\cdot$ leads to C_3H_6 and C_2H_5 radicals) and the formation of
57
58
59
60

pentenes from peroxy radicals by HO_2 -eliminations are favored and less OH radicals are produced via branching reactions.

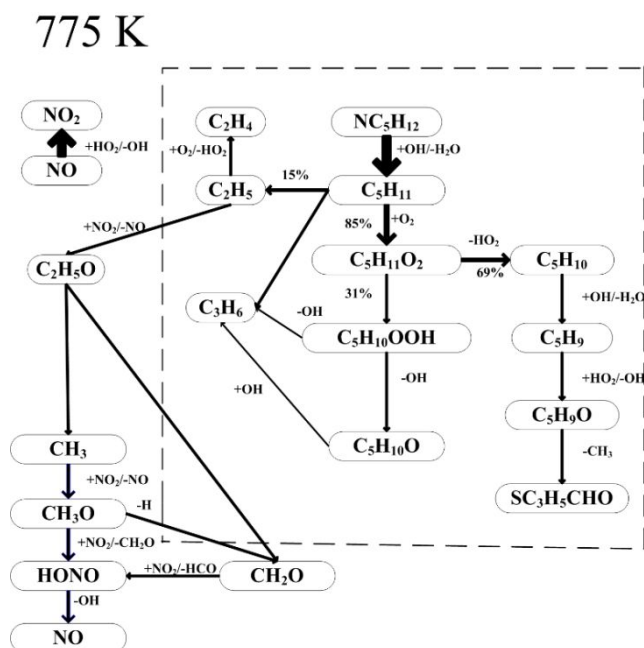


Figure 6: Reaction path diagram for n -pentane oxidation with NO addition at 775 K. The reaction paths, which are included in the dash box, belong to the common n -pentane consumption routes with or without NO_x addition. Only the decomposition pathways deriving from C_5H_{11} -2 are shown.

When added, NO can react with HO_2 radicals releasing OH radical and promoting n -pentane oxidation. C_2H_5 radical, produced from pentyl radical decomposition, could further react with O_2 to form C_2H_4 and HO_2 , creating a second abundant source of this last radical. This is the reason why the n -pentane conversion in the presence of NO is faster than that in the case of neat n -pentane oxidation. To a lower extent, a similar trend is observed when NO_2 is added. Although, since NO is not present as a reactant, it is only produced by reactions of NO_2 with $\text{C}_2\text{H}_5\text{O}$ or CH_3O radicals, which can react with HO_2 and be a source of OH radicals.

With respect to the HONO, in both NO and NO_2 cases, the main reaction routes are similar as mentioned at 725 K. However, the HONO dissociation reaction ($\text{HONO} + \text{M} = \text{OH} + \text{NO} + \text{M}$) is

1 favored by the relative high temperature. The released OH radical could enhance the *n*-pentane
2 oxidation as well.
3
4

5
6 Moreover, first-order sensitivity analyses were performed under the conditions of Figure 2 (Ar
7 as bath gas) at 625 and 775 K. The sensitivity coefficients for *n*-pentane mole fractions are displayed
8 in Figure 7. In this figure, reactions promoting *n*-pentane oxidation are indicated by negative sensitivity
9 coefficients. Because at 625 K, in the presence of NO, no *n*-pentane consumption was observed in
10 both experimental and model points of view, no sensitivity analysis is presented at this temperature
11 with added NO.
12
13
14
15
16
17
18
19

20 For neat *n*-pentane, at 625 K, the reactions associated with OH radicals attacking *n*-pentane
21 and leading to 1- and 2-pentyl radicals show the strongest negative sensitivity coefficients on *n*-pentane
22 mole fraction, along with the addition to O₂ of the main hydroperoxypentyl radical obtained from
23 2-pentyl radicals, which is the main source of the OH radicals. Note that the H-abstractions leading to
24 3-pentyl radicals have some inhibiting effect. This is because the peroxy radicals obtained from
25 3-pentyl radicals isomerise less easily than those obtained from 1- and 2-pentyl radicals. The formation
26 pathways of pentenes and HO₂ radicals inhibit the *n*-pentane oxidation, which is consistent with the
27 reaction path analysis.
28
29
30
31
32
33
34
35
36
37
38

39 Figure 6 shows that, in presence of NO₂, at 625 K, the reactions involving HO₂ radicals are
40 particularly influential. In agreement with the flow rate analysis, the reaction of HO₂ radicals with NO
41 to produce OH radicals has a strong promoting effect. The consumption by NO of the peroxy radicals
42 deriving from 2-pentyl radicals to give alkoxy radicals has a significant inhibiting influence.
43
44
45
46
47
48
49
50
51
52
53
54
55
56
57
58
59
60

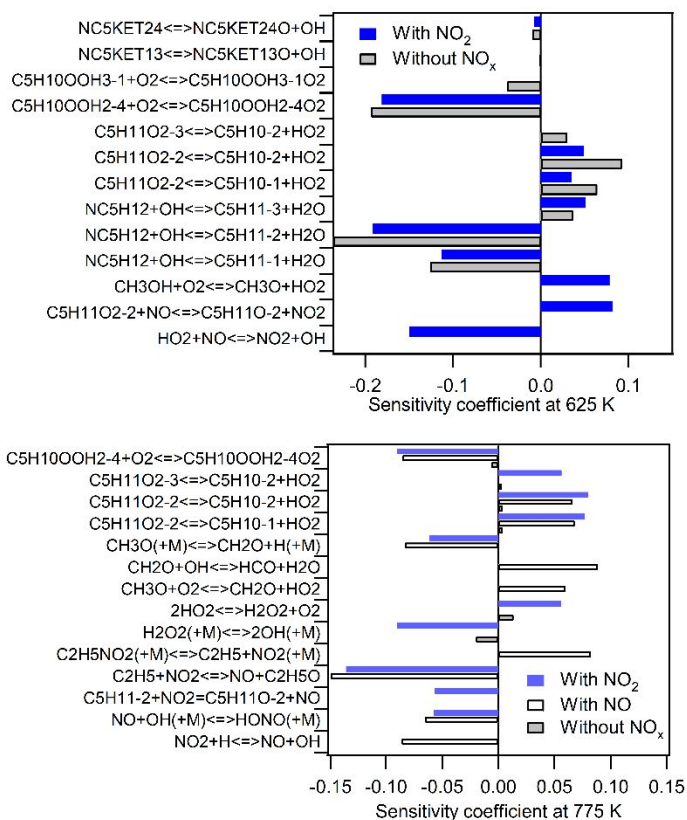


Figure 7: Sensitivity coefficient for *n*-pentane mole fraction at 625 K and 775 K for neat *n*-pentane oxidation and in presence of NO₂ or NO (only top 10 sensitive reactions are displayed).

At 775 K, the NO₂-NO conversion reaction induced by C₂H₅ radical (C₂H₅+NO₂=NO+C₂H₅O) has a strong promoting effect on the *n*-pentane oxidation in the presence of both NO and NO₂. This effect is combined with that of the reactions releasing OH radicals or H atoms, such as NO₂+H=NO+OH, NO+OH+M=HONO+M, H₂O₂+M=2OH+M, and CH₃O+M=CH₂O+H+M, as is shown by their large sensitivity coefficients.

Figure 8 presents the sensitivity analysis for HONO mole fraction at 625 K and 775 K. Positive coefficients indicate reactions favoring HONO formation. Because at 625 K, in the presence of NO, no HONO formation was reported in both experiments and modeling, no HONO sensitivity analysis is displayed at this temperature with added NO.

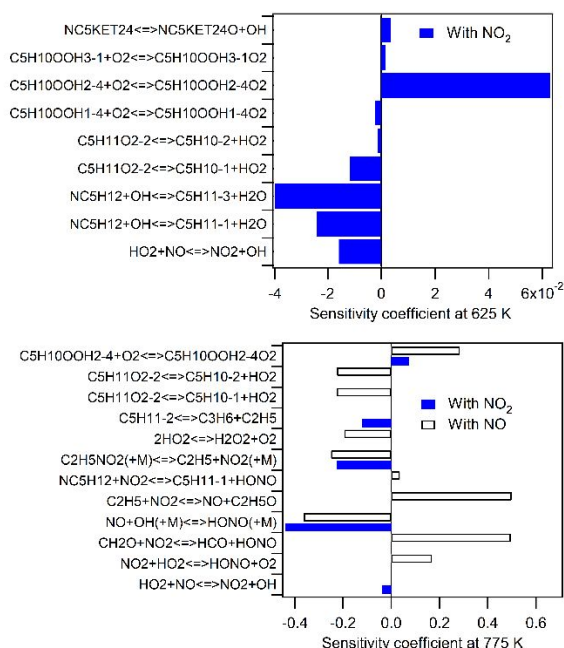


Figure 8: Sensitivity coefficient for HONO mole fraction at 625 K and 775 K for neat *n*-pentane oxidation and in presence of NO₂ or NO (only top 10 sensitive reactions are displayed).

At 625 K, in presence of NO₂, the most significant HONO reaction promoting formation is the addition to O₂ of the main hydroperoxypentyl radical obtained from 2-pentyl radicals. This is because this reaction favors the overall reactivity, but more especially because it leads to the formation of the ketohydroperoxides, the decomposition of which is the source of CH₃O radicals. The reaction of these last radicals with NO₂ is responsible for more than 80% of HONO formation at this temperature. The H-abstractions from *n*-pentane competing with the formation of 2-pentyl radicals have a negative influence on HONO formation.

At 775 K, both with NO and NO₂ addition, again the addition to O₂ of the main hydroperoxypentyl radical obtained from 2-pentyl radicals shows a notable sensitivity towards HONO formation. The reactions associated with C₂H₅O, a precursor of CH₃O radicals, CH₂O and HO₂ radicals play an important role in promoting HONO formation. The HONO decomposition has the strongest depleting influence on the nitrogenated species.

5. Conclusions

This work presents an investigation of the oxidation of *n*-pentane in a jet-stirred reactor from both experimental and modeling points of view. Experiments were carried out at 107 kPa and temperatures between 500 and 1100 K with a fixed residence time of 2.0 s under stoichiometric conditions. The effects of different bath gases (He, Ar, CO₂) as well as NO₂ and NO in Ar on fuel reactivity were studied. Note that HONO quantification was performed with the help of cw-CRDS. In general, there is a good agreement between experimental results and model predictions.

The obtained experimental results are almost identical with the different kinds of bath gases in low temperature oxidation. Above 800 K, the fuel reactivity is affected by the bath gas in the order CO₂ > Ar > He. With CO₂ as a carrier gas, CO formation is larger than those with the He and Ar as carrier gases. Moreover, the addition of NO₂ produces also comparable results, except for the largest conversion of *n*-pentane when temperature is above 700 K. On the contrary, in the presence of NO, we observed a significant delay of the initial temperature for the start of *n*-pentane oxidation. The onset temperatures of HONO formation in the presence of NO₂ and NO are 575 K and 650 K, respectively.

Kinetic analysis showed that the different behaviors of NO and NO₂ addition on *n*-pentane oxidation are related to their roles in the NO_x sub-mechanism. As for NO, the C₅H₁₁O₂+NO = C₅H₁₁O+NO₂ reaction alters the main route of C₅H₁₁O₂ consumption leading to chain-branching at low temperature, and therefore strongly hinders the reactivity of the system. With respect to NO₂, the NO₂+CH₃=NO+CH₃O reaction is responsible for the NO₂ consumption and has a less directly relevant effect on low temperature *n*-pentane oxidation. This can account for the diverse *n*-pentane oxidation behavior with NO and NO₂ addition. The reactions associated with NO₂ and CH_iO (i=2,3) are mainly responsible for the HONO formation, regardless of NO or NO₂ addition, the reverse of OH+NO+M=HONO+M reaction is the major source of HONO depletion.

An extension of this work at higher pressures and for various fuels (e.g. *n*-heptane) or biofuels would certainly be of interest.

Acknowledgements

This work has received funding the COST Action CM1404 “Chemistry of smart energy carriers and technologies”. Dr Marrodán acknowledges Aragón Government for the predoctoral grant awarded.

Prof. Ju thanks Université de Lorraine for his invited visit to Nancy and the support from Army Research Office with grant number W911NF-16-1-0076 at Princeton.

References

- (1) Kalghatgi, G. T. *Proc. Combust. Inst.* **2015**, 35, (1), 101-115.
- (2) Liu, F.; Guo, H.; Smallwood, G. J.; Gülder, Ö. L. *Combust. Flame* **2001**, 125, (1), 778-787.
- (3) Giménez-López, J.; Millera, A.; Bilbao, R.; Alzueta, M. U. *Combust. Flame* **2010**, 157, (2), 267-276.
- (4) Anderlohr, J. M.; Pires da Cruz, A.; Bounaceur, R.; Battin-Leclerc, F. *Combust. Sci. Technol.* **2010**, 182, (1), 39-59.
- (5) Abián, M.; Giménez-López, J.; Bilbao, R.; Alzueta, M. U. *Proc. Combust. Inst.* **2011**, 33, (1), 317-323.
- (6) Schönborn, A.; Sayad, P.; Konnov, A. A.; Klingmann, J. *Combust. Flame* **2013**, 160, (6), 1033-1043.
- (7) Sabia, P.; Lubrano Lavadera, M.; Giudicianni, P.; Sorrentino, G.; Ragucci, R.; de Joannon, M. *Combust. Flame* **2015**, 162, (3), 533-543.
- (8) Sabia, P.; Lubrano Lavadera, M.; Sorrentino, G.; Giudicianni, P.; Ragucci, R.; de Joannon, M. *Flow, Turbu. Combust.* **2016**, 96, (2), 433-448.
- (9) Lubrano Lavadera, M.; Sabia, P.; Sorrentino, G.; Ragucci, R.; de Joannon, M. *Fuel* **2016**, 184, 876-888.
- (10) Di, H.; He, X.; Zhang, P.; Wang, Z.; Wooldridge, M. S.; Law, C. K.; Wang, C.; Shuai, S.; Wang, J. *Combust. Flame* **2014**, 161, (10), 2531-2538.
- (11) Zhang, X.; Ye, W.; Shi, J. C.; Wu, X. J.; Zhang, R. T.; Luo, S. N. *Energy Fuels* **2017**, 31, (11), 12780-12790.
- (12) Mathieu, O.; Pemelton, J. M.; Bourque, G.; Petersen, E. L. *Combust. Flame* **2015**, 162, (8), 3053-3070.
- (13) Sivaramakrishnan, R.; Brezinsky, K.; Dayma, G.; Dagaut, P. *Phys. Chem. Chem. Phys.* **2007**, 9, (31), 4230-4244.
- (14) Herzler, J.; Naumann, C. *Combust. Sci. Technol.* **2012**, 184, (10-11), 1635-1650.
- (15) Gokulakrishnan, P.; Fuller, C. C.; Klassen, M. S.; Joklik, R. G.; Kochar, Y. N.; Vaden, S. N.; Lieuwen, T. C.; Seitzman, J. M. *Combust. Flame* **2014**, 161, (8), 2038-2053.
- (16) Bromly, J. H.; Barnes, F. J.; Muris, S.; You, X.; Haynes, B. S. *Combust. Sci. Technol.* **1996**, 115, (4-6), 259-296.
- (17) Alzueta, M. U.; Glarborg, P.; Dam-Johansen, K. *Combust. Flame* **1997**, 109, (1), 25-36.
- (18) Glarborg, P.; Alzueta, M. U.; Dam-Johansen, K.; Miller, J. A. *Combust. Flame* **1998**, 115, (1-2), 1-27.
- (19) Bendtsen, A. B.; Glarborg, P.; Dam-Johansen, K. I. M. *Combust. Sci. Technol.* **2000**, 151, (1), 31-71.

- 1
2 (20) Dagaut, P.; Luche, J.; Cathonnet, M. *Proc. Combust. Inst.* **2000**, 28, (2), 2459-2465.
3 (21) Dagaut, P.; Nicolle, A. *Combust. Flame* **2005**, 140, (3), 161-171.
4 (22) Rasmussen, C. L.; Rasmussen, A. E.; Glarborg, P. *Combust. Flame* **2008**, 154, (3), 529-545.
5 (23) Mendiara, T.; Glarborg, P. *Energy Fuels* **2009**, 23, (7), 3565-3572.
6 (24) Chan, Y. L.; Barnes, F. J.; Bromly, J. H.; Konnov, A. A.; Zhang, D. K. *Proc. Combust. Inst.*
7 **2011**, 33, (1), 441-447.
8 (25) Giménez-López, J.; Aranda, V.; Millera, A.; Bilbao, R.; Alzueta, M. U. *Fuel Proc. Technol.*
9 **2011**, 92, (3), 582-589.
10 (26) Chan, Y.; Bromly, J.; Konnov, A.; Zhang, D. *Combust. Sci. Technol.* **2012**, 184, (1), 114-132.
11 (27) Zhang, J.; Burklé-Vitzthum, V.; Marquaire, P.-M. *Combust. Sci. Technol.* **2015**, 187, (7), 1139-
12 1156.
13 (28) Chakir, A.; Belumam, M.; Boettner, J. C.; Cathonnet, M. *Combust. Sci. Technol.* **1991**, 77, (4-
14 6), 239-260.
15 (29) Simon, V.; Simon, Y.; Scacchi, G.; Baronnet, F. *Can. J. Chem.* **1997**, 75, (5), 575-584.
16 (30) Bugler, J.; Rodriguez, A.; Herbinet, O.; Battin-Leclerc, F.; Togbé, C.; Dayma, G.; Dagaut, P.;
17 Curran, H. J. *Proc. Combust. Inst.* **2017**, 36, (1), 441-448.
18 (31) Rodriguez, A.; Herbinet, O.; Wang, Z.; Qi, F.; Fittschen, C.; Westmoreland, P. R.; Battin-
19 Leclerc, F. *Proc. Combust. Inst.* **2017**, 36, (1), 333-342.
20 (32) Marks, B.; Mathieu, O.; Archuleta, R.; Petersen, E.; Metcalfe, W.; Curran, H.; Bourque, G. In
21 *51st AIAA Aerospace Sciences Meeting including the New Horizons Forum and Aerospace*
22 *Exposition, American Institute of Aeronautics and Astronautics: 2013.*
23 (33) Bugler, J.; Marks, B.; Mathieu, O.; Archuleta, R.; Camou, A.; Grégoire, C.; Heufer, K. A.;
24 Petersen, E. L.; Curran, H. J. *Combust. Flame* **2016**, 163, 138-156.
25 (34) Zhukov, V. P.; Sechenov, V. A.; Starikovskii, A. Y. *Combust. Flame* **2005**, 140, (3), 196-203.
26 (35) Jin, H.; Pieper, J.; Hemken, C.; Bräuer, E.; Ruwe, L.; Kohse-Höinghaus, K. *Combust. Flame*
27 **2018**, 193, 36-53.
28 (36) Prabhu, S. K.; Bhat, R. K.; Miller, D. L.; Cernansky, N. P. *Combust. Flame* **1996**, 104, (4), 377-
29 390.
30 (37) Glaude, P. A.; Marinov, N.; Koshiishi, Y.; Matsunaga, N.; Hori, M. *Energy Fuels* **2005**, 19, (5),
31 1839-1849.
32 (38) Zhao, H.; Wu, L.; Patrick, C.; Zhang, Z.; Rezugui, Y.; Yang, X.; Wysocki, G.; Ju, Y. *Combust.*
33 *Flame* **2018**, 197, 78-87.
34 (39) Zhao, H.; Dana, A. G.; Zhang, Z.; Green, W. H.; Ju, Y. *Energy* **2018**, 165, 727-738.
35 (40) Perner, D.; Platt, U. *Geophys. Res. Lett.* **1979**, 6 (12), 917-920.
36 (41) Karlsson, R. S.; Ljungstrom, E. B. *Environ. Sci. Technol.* **1996**, 30 (6), 2008-2013.
37 (42) Jain, C.; Morajkar, P.; Schoemaeker, C.; Viskolcz, B.; Fittschen, C. *J. Phys. Chem. A* **2011**,
38 115, (39), 10720-10728.
39 (43) Chai, J.; Goldsmith, C. F. *Proc. Combust. Inst.* **2017**, 36, (1), 617-626.
40 (44) Song, Y.; Marrodán, L.; Vin, N.; Herbinet, O.; Assaf, E.; Fittschen, C.; Stagni, A.; Faravelli, T.;
41 Alzueta, M. U.; Battin-Leclerc, F. *Proc. Combust. Inst.* **2018**, 37, (1), 667-675.
42 (45) Marrodán, L.; Song, Y.; Herbinet, O.; Alzueta, M. U.; Fittschen, C.; Ju, Y.G.; Battin-Leclerc, F.
43 *Chem. Phys. Lett.* **2019** in press: doi.org/10.1016/j.cplett.2019.01.038
44 (46) Herbinet, O.; Battin-Leclerc, F. *Int. J. Chem. Kinet.* **2014**, 46, (10), 619-639.
45 (47) Bahrini, C.; Herbinet, O.; Glaude, P.-A.; Schoemaeker, C.; Fittschen, C.; Battin-Leclerc, F.
46 *Chem. Phys. Lett.* **2012**, 534, 1-7.
47 (48) Anderlohr, J. M.; Bounaceur, R.; Pires Da Cruz, A.; Battin-Leclerc, F. *Combust. Flame* **2009**,
48 156, (2), 505-521.
49 (49) Glarborg, P.; Bendtsen, A.B.; Miller, J.A. *Int. J. Chem. Kinet.* **1999**, 31, 591-602
50 (50) Atkinson, R.; Baulch, D. L.; Cox, R. A.; Jr., R. F. H.; Kerr, J. A.; Troe, J. *J. Phys. Chem. Ref.*
51 *Data* **1992**, 21, (6), 1125-1568.
52
53
54
55
56
57
58
59
60

- 1
2 (51) Tsang, W.; Herron, J. T. *J. Phys. Chem. Ref. Data* **1991**, 20, (4), 609-663.
3 (52) Glaude, P. A.; Conraud, V.; Fournet, R.; Battin-Leclerc, F.; Côme, G. M.; Scacchi, G.; Dagaut,
4 P.; Cathonnet, M. *Energy Fuels* **2002**, 16, (5), 1186-1195.
5 (53) Chan, W.-T.; Heck, S. M.; Pritchard, H. O. *Phys. Chem. Chem. Phys.* **2001**, 3, (1), 56-62.
6 (54) Choi, Y. M.; Lin, M. C. *Int. J. Chem. Kinet.* **2005**, 37, (5), 261-274.
7 (55) Atkinson, R.; Baulch, D. L.; Cox, R. A.; Crowley, J. N.; Hampson, R. F.; Hynes, R. G.; Jenkin,
8 M. E.; Rossi, M. J.; Troe, J. *Atmos. Chem. Phys.* **2004**, 4, (6), 1461-1738.
9 (56) Burkholder, J. B.; Mellouki, A.; Talukdar, R.; Ravishankara, A. R. *Int. J. Chem. Kinet.* **1992**,
10 24, (8), 711-725.
11 (57) CHEMKIN-PRO 15151, Reaction Design, San Diego, **2013**.
12 (58) Lubrano Lavadera, M.; Song, Y.; Sabia, P.; Herbinet, O.; Pelucchi, M.; Stagni, A.; Faravelli, T.;
13 Battin-Leclerc, F.; de Joannon, M. *Energy Fuels* **2018**, 32, (10), 10088-10099.
14 (59) P.J. Linstrom and W.G. Mallard, Eds., NIST Chemistry WebBook, NIST Standard Reference
15 Database Number 69, National Institute of Standards and Technology, Gaithersburg MD,
16 20899, <https://doi.org/10.18434/T4D303>
17
18
19
20
21
22
23
24
25
26
27
28
29
30
31
32
33
34
35
36
37
38
39
40
41
42
43
44
45
46
47
48
49
50
51
52
53
54
55
56
57
58
59
60